Seismic and aseismic slip in EGS reservoir: an experimental approach

J. Schmittbuhl[1], O. Lengliné[1], Zaepfel[1], F. Cornet[1], N. Cuenot[2] and A. Genter[2].

[1] EOST, Université de Strasbourg/CNRS, 5 rue René Descartes, 67084 Strasbourg Cedex, France

[2] GEIE EMC, Route de Soultz-sous-Forêts, Kutzenhausen, France

Jean.Schmittbuhl@unistra.fr

Keywords: induced seismicity, brittle creep, analogue modelling, aseismic deformations, EGS.

ABSTRACT

Observations in EGS reservoirs of induced seismicity and slow propagating ruptures on related faults suggest a close link between the two phenomena. Here we present laboratory experiments that explore, in great detail, the deformation processes of heterogeneous interfaces in the brittle-creep regime. We track the evolution of an interfacial crack over 7 orders of magnitude in time and 5 orders of magnitude in space using optical and acoustic sensors. We show that seismic event occurrences in time and space are in strong relation with the development of the aseismic motion recorded during the experiments. We also infer the statistical properties of the organization of the seismicity that show strong space-time clustering. We finally link our results to the seismicity recorded during hydraulic stimulation in the Soultz-sous-Forêts deep geothermal reservoir in order to show how aseismic processes drive this seismicity with little effects of the fluid pressure.

1. INTRODUCTION

The exploitation of a geothermal reservoir can lead to the occurrence of an abundant seismicity, particularly during phases of hydraulic stimulation. This seismicity has a strong societal impact, as it can be felt by the population, especially in densely populated area as in Europe e.g. M_L=3.4, Basel, 2006 (Häring et al, 2006). Reducing this impact is thus one of the main challenges in the development of geothermal energy production. In order to understand the mechanical processes responsible for seismic activity, we studied the link between earthquakes and aseismic deformations. Deciphering this link between seismicity and aseismic motion can not only help to mitigate the risk posed by seismicity but also can help to monitor and model the evolution of the geothermal reservoir. The mechanism relating earthquakes and aseismic processes is still elusive due to the difficulty of imaging these phenomena of large spatiotemporal variability at depth. However, a good example of joint seismic and aseismic deformation has been obtained at the EGS site of Soultz-sous-Forêts (France) (Genter et al, 2010) in particular during the 1993 water injection experiment into a naturally fractured granite.

1.1 Aseismic slip at Soultz-sous-Forêts

Aseismic slips were first observed at Soultz-sous-Forêts by Cornet et al (1997). They showed that during the stimulation of GPK1 in 1993, the borehole has been shifted at several depths just below the casing shoe at 2857m. From ultrasonic borehole images between 2853m and 3104m before and after the hydraulic injection of 44000 m^3, they evidenced fresh displacements along existing fractures between 2867m and 2976m that were of the order of several millimetres to several centimeters. One of the largest offset was measured at 2925m: 4.3cm and considered as part of significant fault of the reservoir with a quasi-vertical fault (dip of 86° and a dip direction of N48). Interestingly this fault zone is not part of the major fault zones observed during borehole logging (Sausse et al, 2010) An important complementary observation is the seismicity recorded during the injection period corresponding to the occurrence of the borehole offset. Indeed, 165 events were recorded from the surface network which was far much less that the number of events recorded by the borehole down-hole network (20000 events). They showed however that the magnitude of the largest recorded event was M_L=1.9 corresponding to a seismic moment M_0 of 5.4 10^{11} Nm and an rupture area of typically d=50m for a stress drop of 9 MPa (assuming a circular crack embedded in an elastic isotropic medium and a shear modulus of μ=20 GPa) consistently with observations in similar context (Abercrombie, 1993). From general scaling laws (Kanamori and Anderson, 1975), the expected slip D from this largest event would be of the order of one centimeter: $D=4M_0/\pi\mu d^2$ which is significantly smaller than the measured offset in the borehole. Cornet et al, (1997) concluded that the large slips evidenced in the borehole could not be explained by the recorded earthquakes. Subsequently, they proposed that these large slips are aseismic which was the first indirect observation of aseismic slip at Soultz-sous-Forêts EGS induced by a fluid injection.

1.2. Micro-seismicity during aseismic slip at Soultz-sous-Forêts

Ten years later, Bourouis and Bernard (2007) re-explored these outstanding observations trying to conduct a fine analysis of the micro-seismicity during the injection period. They used a multiplet approach

and relocated up to 400 events within the fault zone where aseismic slip was observed. The location accuracy was of the order of 1m and they obtained 30 multiplets or families of similar events within the fault zone. An interesting observation is that the rupture size for all these events is of the order of d=10m. From their observations, they inferred three important conclusions. First events within a multiplet were located within the same rupture zone which showed that the same asperity was reloaded and broken several times during the injection period. The second conclusion is that several asperities along the fault were ruptured at the same time during the injection. Third, the cumulative slip of each asperity through several ruptures was consistent with the borehole offset measurement. The conclusion is a clear image of the fault behaviour during loading: the fault undergoes a large aseismic slip which triggers multiple local asperity failure.

The goal of the present paper is to propose a mechanical model of this fault behaviour. We develop an experimental approach to mimic the response of a single fault when submitted to a slow rupture propagation but locally unstable at asperities which are responsible for micro seismic activity. The model is analogous to incorporate the large space and time dynamics: 7 orders of magnitude in time and 5 orders of magnitude in space. A numerical approach would be difficult with such large range of timescales and wavelengths (Kaneko et al, 2010).

2. EXPERIMENTAL APPROACH

2.1 An analogous fault with random asperities

Samples are made of transparent Plexiglas and accordingly provide optical access to the rupture propagation. The analogous fault is obtained by annealing two plates of 20x10x1cm^3 and 23x2.8x0.5 cm^3 at 190°C during 45 min which is significantly above the glass transition of the material but below the melting point. With some normal load, the two plates get in close contact and stick together along a relatively weak plane (weaker than the bulk) (Schmittbuhl and Maloy, 1997). The goal is to study the collective behavior of multiple asperities. To do so, we sandblast one of the plates before the annealing procedure (see Figure 1) to induce local toughness fluctuations (Lengliné et al, 2011a).

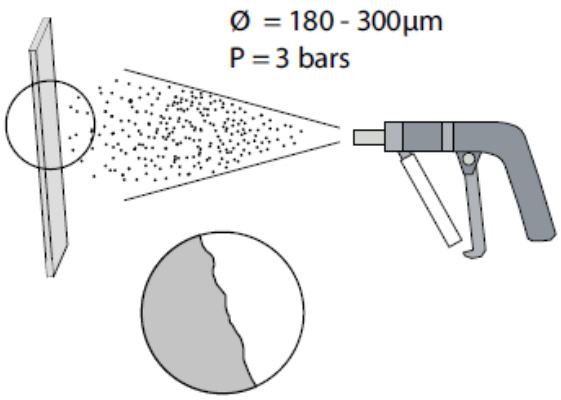

Figure 1: Sandblasting of one of the plate surface to introduce small topography fluctuations that will induce local toughness fluctuations during the annealing procedure.

2.2 A subcritical rupture propagation

Samples with a weak plane along which the toughness is fluctuating but with an average toughness, lower than that of the bulk, are submitted to a Cantilever loading (mode I), (see Figure 2) (Lengliné et al, 2012).

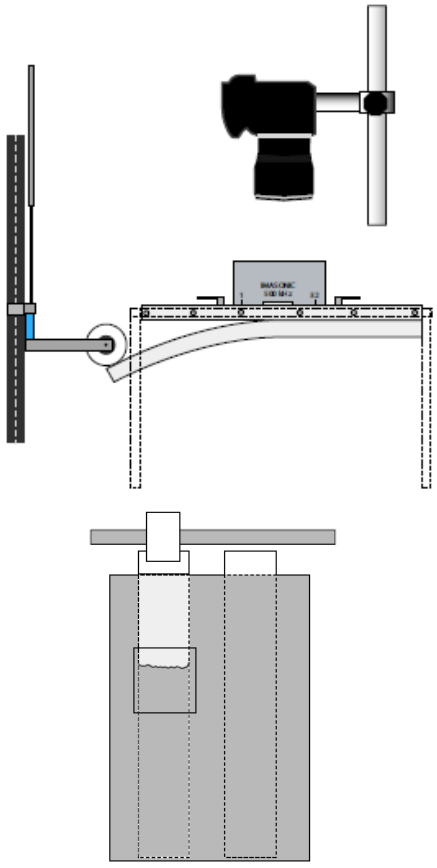

Figure 2: Experimental setup: a) side view. Samples are made of two plates that are annealed together. One of the plates is longer and undergoes a Cantilever load from the vertical displacement of a rod (white circle) that bends the plate. This bending with respect to the other plate induces a mode I fracture that propagates along the weak annealing interface. A camera is sitting over the

sample and takes optical image of the front propagation. Acoustic sensors are also attached to the fixed plate and record acoustic emissions during propagation. b) Top view of the sample. The white rod is loading the sample. Light gray area corresponds to the broken zone behind the fracture front. The black square shows the zone where pictures are taken.

The loading includes different phases: first the plate is loaded at a low constant speed of the rod up to the initiation of the fracture and its propagation over a few millimetres at quasi constant velocity. The loading rate is of the order of a millimeter per second. The setup being at imposed displacement, the crack propagation is stable and the average rupture velocity is controlled by the loading rate in the subcritical regime. Second the loading rate is set zero and the fracture propagates only owing to the relaxation of the rupture at a decreasing speed (Lengliné et al, 2011b).

2.2 Optical monitoring of the fracture front

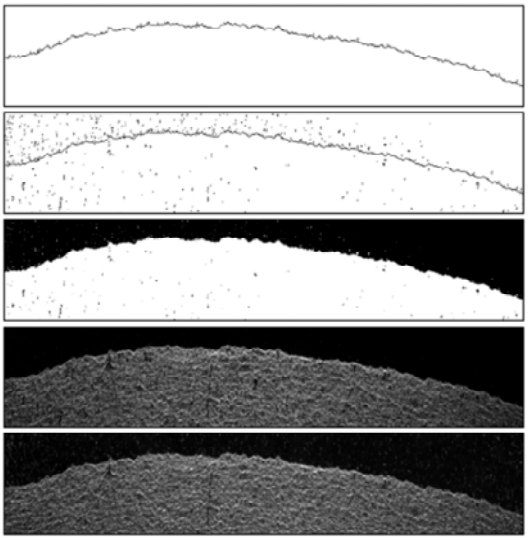

Figure 3: Image of the fracture propagation from bottom to top. The cracked area is in light gray. The scale is given by the size of the image which covers a region of 1.3cm. Each pixel corresponds to an area of 20x20µm^2. From image treatment allows a precise description of the fracture front (top view) for each image showing the details of the pinning of the front on the local asperities corresponding to local increase of the toughness. Using a series of image, one can reproduce the exact history of the fracture front trough time.

Taking images at high resolution (from 1Mpixels with the fast camera up to 12 Mpixel with the SLR Digital camera) we can obtain a precise spatial description of the fracture front (see Figure 3). It is observed that Fourier analysis of the front shows a power law behavior of the power spectrum over more than two decades (see Figure 4) with a roughness exponent H=0.6 (Schmittbuhl and Maloy, 1997, Schmittbuhl et al, 2003; Lengliné et al, 2011a).

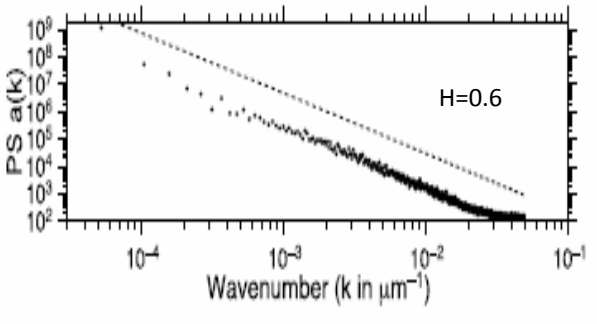

Figure 4: Average power spectrum of the fracture front showing a power law exponent consistent with a roughness exponent H=0.6.

2.3 Acoustic emissions during fracture propagation

From acoustic sensors, acoustic emissions are recorded at 5Msamples/sec during up to 30 sec (cf the duration of each experiment). As a first step we extract major acoustic signals and correlate them with advances of the front observed from the optical acquisition. Figure 5 shows an example of such an event. The fast camera was set at a frame rate of 1000 images/sec with a time delay between images of 1ms. During that period, an acoustic event with a significantly much smaller source duration (around 100µs) has been triggered. This is a first direct observation of a simultaneous aseismic and seismic deformation, the aseismic event observed by the optical camera lasting significantly longer than the acoustic event.

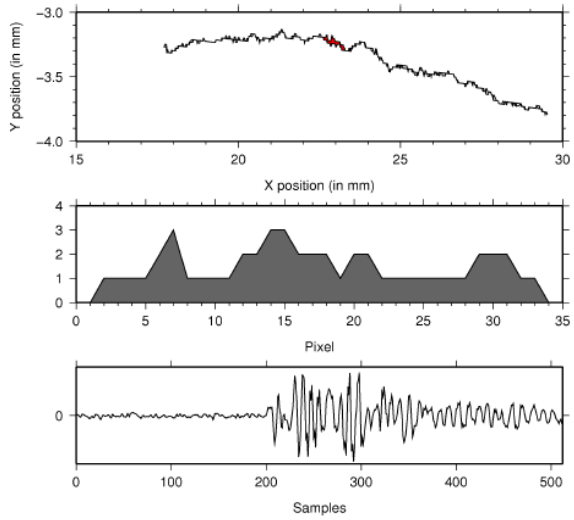

Figure 5: Optical and acoustical description of a major event during the propagation. Top view: superimposition of front between two consecutive optical images. In red is shown the area of the event. Middle view: detail of the crack advance (dt=1ms): Bottom view: waveform of the acoustic emission recorded by one of the acoustic sensor. The duration of the event is of the order of 200µs.

During each experiment, i.e. the propagation of the fracture front over several millimetres, we recorded several hundreds of acoustic emissions. Figure 6 shows a distribution of the energy recorded for each

event. A calibration provides an estimate of the absolute energy of the order of 10^{-10} to 10^{-8}J per events consistent with magnitudes in the range -10 to -8 using the classical energy-magnitude relation from Kanamori and Anderson (1975): M = 2/3Log(E) – 3.2. Figure 6 shows that a power law behaviour exists over two decades of energy with a slope consistent with Gutenberg-Richter distribution.

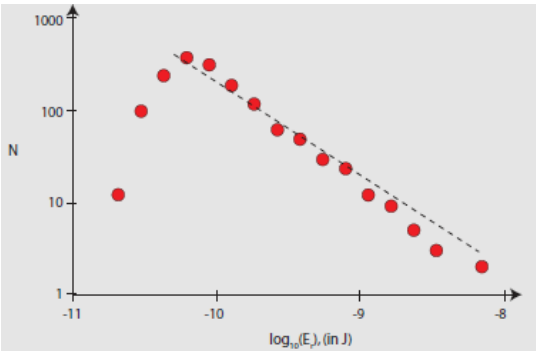

Figure 6: Distribution of the acoustic emission energy during an experiment. The power law behavior shows the large range of energy scales and is consistent with a Gutenberg-Richter distribution.

2.4 Combining optical (aseismic) and acoustical (seismic) information

An on-going work is about the location of acoustic events not from a correlation with the location of optical events but from the inversion of the acoustic arrivals (time picking of the phases). Because of the large number of waveforms (up to 64 sensors) and the continuous recording at very high frequency (5 MHz), we introduced an automatic picking algorithm based on array analysis. An example of the location of one event is shown in Figure 7.

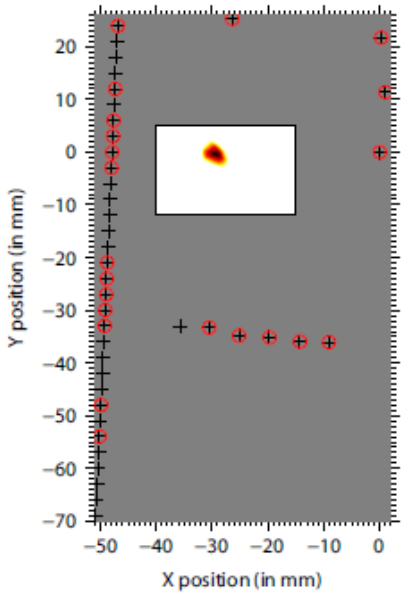

Figure 7: Illustration of the acoustic location from inversion of the waveforms. Red circles show the active sensors during the experiment and their relative position to the zone observed by the camera (white rectangle). The coloured zone is the probability distribution estimated from the cost function of the minimization during the inversion.

Figures 8 and 9 show the evolution of the locations of the acoustic emissions during one experiment where the fracture front advances by one centimeter. We are able to follow the front advance during its propagation even if the spatial resolution of the acoustic location is significantly larger than the optical resolution.

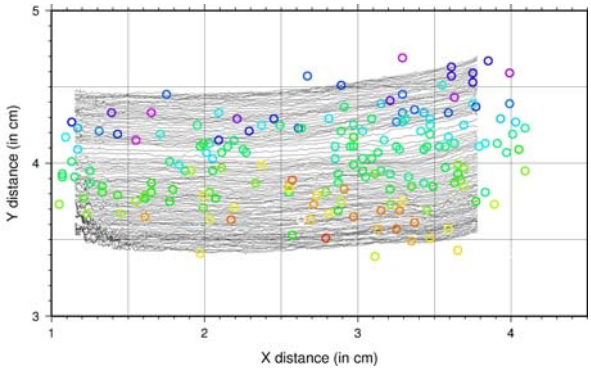

Figure 8: Spatial view of the locations of a set of acoustic emissions (circles) superimposed to the tracking of the rupture front measured by the fast camera. The colour code of the circles shows the time evolution of the acoustic emissions.

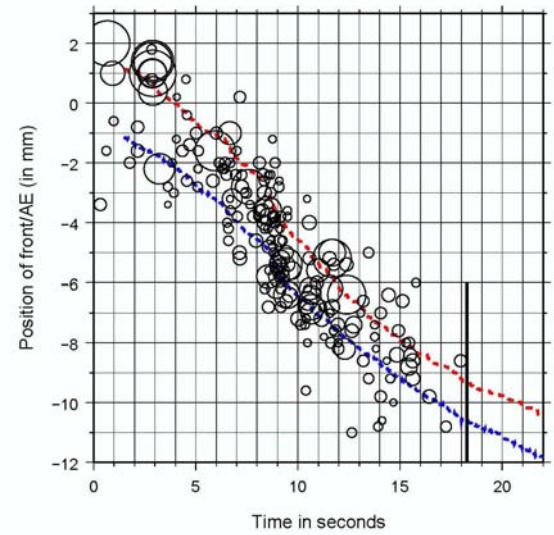

Figure 9: Space-time evolution of the acoustic emissions compared to the front advance: in blue the position of the tip of the front (i.e. the most advanced part or the front), in red, position of the latest advanced part of the front. Circle radius is related to the magnitude of the event.

Figures 8 and 9 evidence that numerous acoustic emissions are triggered during the subcritical fracture propagation. The link between creep and dynamical rupture leading to acoustic emission, is the pinning of the fracture front on asperities, i.e. zones of larger toughness. It shows that the driving process of the acoustic activity is not a cascade process between seismic events but the slow advance of the crack, analogous of slow slip along the fault.

3. COMBINING ASEISMIC AND SEISMIC EVENTS

3.1 An imposed loading perturbation

To go one step further in understanding the link between acoustic emission and local creep events we took advantage of the experimental configuration to introduce a perturbation in the loading and look for the response of the system. Figure 10 shows how is introduced this perturbation if loading rate as a pulse.

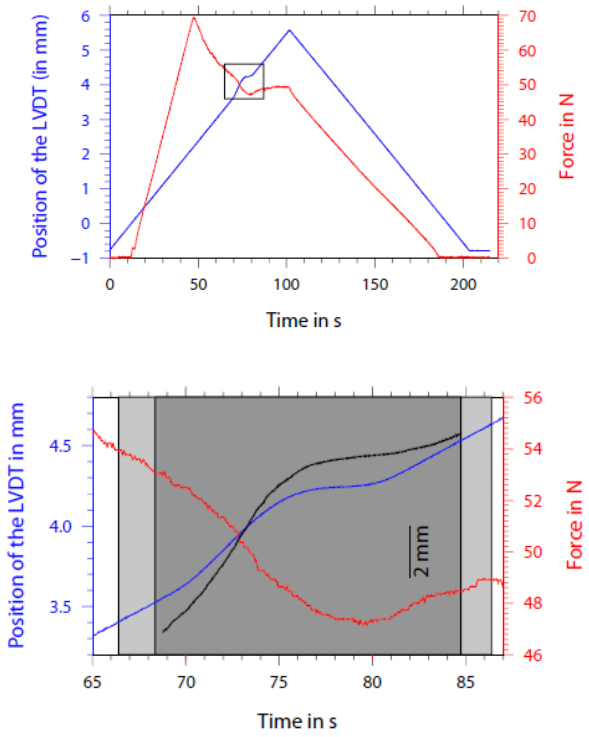

Figure 10: Top panel: loading curve during the whole experiment (blue line). The red line shows the force response. The black box focuses on the detail of the loading perturbation detailed in the bottom panel. Bottom panel: Red and blue curves are the detailed evolution of the loading and the force response shown in top panel around the perturbation. Also presented is the average position of the front (in black with a scale of 2mm).

We observed that the average position of the fracture front follows exactly the perturbation of the loading frame after a small shift in time. The force decreases as the front velocity increases which is a velocity weakening effect.

3.2 Aseismic events

Following the crack front advance with the digital camera as described in section 2, we are able to monitor the local speed of the front (Maloy et al, 2006, Grob et al, 2009). We see that the overall trend of the experiment is imaged by the general evolution of the color: slightly blue at the beginning (long waiting time corresponding to low speed), becoming very red (shorter waiting time corresponding to higher speed) and back to mostly blue during the speed reduction of the front. The interesting part is the detailed of the local velocity. Clearly patches of increased speeds (red patches) exist. By thresholding at ten times the average velocity of the front, the image of the local velocity field, we obtained a set of "optical" events that are significantly faster than the loading speed but also significantly slower than the dynamical rupture velocity (i.e. Rayleigh speed). These zones correspond to aseismic events which are accelerated advances compare to the average speed.

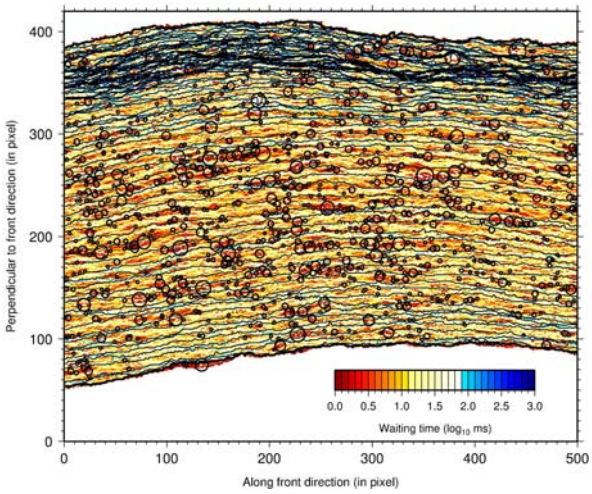

Figure 11: Spatial image of the propagation of the fracture front during a perturbation of the loading. Pixels cover a region of 20x20µm^2. The colour code is the time that the front is waiting at a given pixel (waiting time) which is inversely proportional to the local speed of the front. Circles mark "optical" events made of accelerated patches with respect to the average speed of the front.

An interesting observation is that local velocities are distributed as a unique power law on a broad range of velocities (more than three orders of magnitude): $P(v) \sim v^{-2.55}$ (Maloy et al, 2006), suggesting that most of the energy is dissipated by creep events consistently with Kanamori and Anderson (1975) observations that the radiated energy is always negligible in front of the seismic moment ($M_0/E \approx 1/20000$ where M_0 is the seismic moment describing the total dissipated energy and E the radiated energy).

3.2 When seismic events follow creeping activity

The last input from the experiment is the comparison of the optical events and acoustic emissions during the load perturbation. Figure 12 shows how both families of events are synchronous which clearly suggest that acoustic emissions are directly controlled by the large scale creeping process.

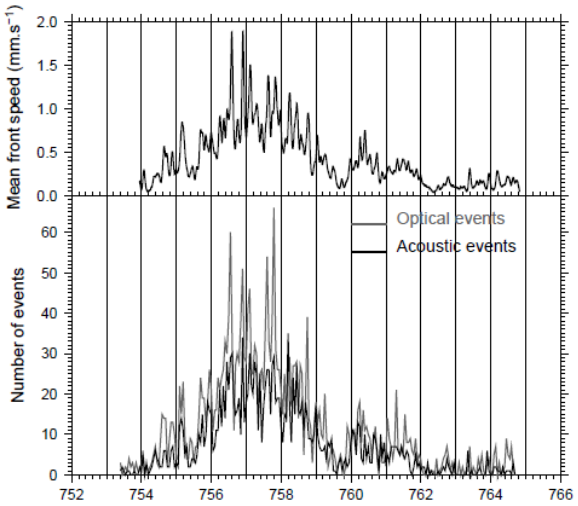

Figure 12: Top panel: Evolution of the average velocity of the fracture front trough time (in sec). The front velocity shows a long period pulse plus short period fluctuations. Bottom panel: Comparison of the rate of optical events (i.e. slow rupture) and acoustic events (i.e. fast rupture) during the average front velocity shown in the upper panel.

4. CONCLUSIONS

Observations at Soultz-sous-Forêts of aseismic slips that are synchronous with micro-seismic events located in multiplets (Cornet et al, 1997, Bourouis and Bernard, 2007) suggest that both processes co-exist within the same fault zones during a fluid injection period. Here we proposed an experimental model that directly supports this observation. Our model is built on the interfacial failure along a heterogeneous weak plane and combines creep failure and brittle rupture without fluid. Experimental observations are numerous and consistent with large scale measurements. They provide clear hints on the processes involved at the asperity scale. Our conclusion is therefore that fluids are not necessarily the driving force of the fault activity in terms of pore pressure. They might have rather a role on local creep acceleration.

REFERENCES

Abercrombie, R. and Leary, P.: Source parameters of small earthquakes recorded at 2.5 km depth, Cajon Pass, Southern California: implications for earthquake scaling, *Geophys. Res. Lett.*, **20**, (1993), 1511-1514.

Bourouis, S. and Bernard, P.: Evidence for coupled seismic and aseismic fault slip during water injection in the geothermal site of Soultz (France), and implications for seismogenic transients, *Geophys. J. Int.*, **169**, (2007), 723-732.

Candela, T., F. Renard, F., Bouchon, M., Schmittbuhl, J. and Brodsky E.:. Fault slip distribution and fault roughness. *Geophys. J. Int.*, **187**(2), (2011), 959-968.

Cornet, F.H., Helm, J., Poitrenaud, H. and Etchecopar, A.: Seismic and aseismic slips induced by large-scale fluid injections, *Pure appl. Geophys.*, **150**, (1997), 563-583.

Genter, A., Evans, K., Cuenot, N., Fritsch, D. and Sanjuan, B.: Contribution of the exploration of deep crystalline fractured reservoir of Soultz to the knowledge of enhanced geothermal system (EGS), *C.R. Geoscience*, **342,** (2010), 502-516.

Grob, M., J. Schmittbuhl, J., Toussaint, R., Rivera, L., Santucci, S. and . Måløy K.J.: Quake catalogs from an optical monitoring of an interfacial crack propagation. *PAGEOPH*, **166,** (2009), (5-7):777-799.

Häring, M.O., Schanz, U., Ladner, F. and Dyer, B.C.: Characterisation of the Basel 1 enhanced geothermal system, *Geothermics*, **37,** (2008), 469-495.

Kanamori, H., and Anderson, D.L.: Theoretical basis of some empirical relations in seismology, *B.S.S.A.*, **65,** (1975), 1073-1095.

Kaneko, Y., Avouac, J.P. and Lapusta, N.: Towards inferring earthquake patterns from geodetic observations of interseismic coupling, *Nat. Geosci.*, **3**, 363-369.

Lengliné, O., Elkhoury J.,, Daniel, G., Schmittbuhl, J., Toussaint, R., Ampuero, J.P. and Bouchon, M.: Interplay of seismic and aseismic deformations during earthquake swarms: an experimental approach. *Earth. Plan. Sci. Lett.*, **331-332**, (2012), 215-223.

Lengliné, O., Schmittbuhl, J., Elkhoury, J., Ampuero, J.P., Toussaint, R. and Måløy, K.J.: Down-scaling during brittle-creep experiments. *J. Geophys. Res.*, **116,** (2011a), B08215.

Lengliné, O., Toussaint, R. Schmittbuhl, J., Elkhoury, J., Ampuero, J.P., . Tallakstad, K.T., Santucci, S. and Måløy, K.J.: Average crack front velocity during subcritical fracture. *Phys. Rev. E*, **84**(3), (2011b), :036104.

Måløy, K.J., Santucci, S., Schmittbuhl, J., and R. Toussaint. Local waiting time fluctuations along a randomly pinned crack front. *Phys. Rev. Lett.*, **96**(4), (2006), 045501.

Sausse, J., Dezayes, C., Dorbath, L., Genter, A., Place, J.: 3D model of fracture zonez at Soultz-sous-Forêts based on geological data, image logs, induced microseismicity and vertical seismic profiles, *C.R. Geoscience*, **342**, (2010), 531-545.

Schmittbuhl, J., Delaplace, A., Måløy, K.J., Perfettini, H. and Vilotte, J.P: Slow crack propagation and slip correlations. *PAGEOPH*, (2003), **160**(5-6):961-976.

Schmittbuhl, J. and Måløy K.J.: Direct observation of a self-affine crack propagation. *Phys. Rev. Lett.*, (1997), **78**:3888-3891

Acknowledgements

This work was done in the framework of the ANR SUPNAF and the Labex G-EAU-THERMIE PROFONDE which was funded by the French government under the program “Investissements d'Avenir”.